



Fermi National Accelerator Laboratory

FERMILAB-Conf-96/209-E

CDF

**W and Z Boson Production with Jets and Inclusive Jet Production in  
 $p\bar{p}$  Collisions at  $\sqrt{s} = 1.8$  TeV**

Alfred T. Goshaw

For the CDF Collaboration

*Fermi National Accelerator Laboratory  
P.O. Box 500, Batavia, Illinois 60510*

*Duke University  
Durham, North Carolina 27708-0305*

August 1996

Submitted to the Proceedings of the *XXXIst Rencontres de Moriond, QCD and High Energy Hadronic Interactions*, Les Arcs, France, March 23-30, 1996

### **Disclaimer**

*This report was prepared as an account of work sponsored by an agency of the United States Government. Neither the United States Government nor any agency thereof, nor any of their employees, makes any warranty, expressed or implied, or assumes any legal liability or responsibility for the accuracy, completeness, or usefulness of any information, apparatus, product, or process disclosed, or represents that its use would not infringe privately owned rights. Reference herein to any specific commercial product, process, or service by trade name, trademark, manufacturer, or otherwise, does not necessarily constitute or imply its endorsement, recommendation, or favoring by the United States Government or any agency thereof. The views and opinions of authors expressed herein do not necessarily state or reflect those of the United States Government or any agency thereof.*

**W AND Z BOSON PRODUCTION WITH JETS  
AND INCLUSIVE JET PRODUCTION  
IN  $p\bar{p}$  COLLISIONS AT  $\sqrt{s} = 1.8$  TEV**

Alfred T. Goshaw  
Duke University  
Durham, NC 27708-0305  
For the CDF Collaboration

Submitted to the Moriond Conference Proceedings  
"QCD and High Energy Hadronic Interactions"  
Les Arcs, France  
March 23-30, 1996

**ABSTRACT**

The production properties of jets produced in  $p\bar{p}$  collisions at  $\sqrt{s} = 1.8$  TeV have been measured using the CDF detector. The data are compared to predictions of leading order and next to leading order QCD predictions. Both inclusive jets and those produced in association with W and Z bosons are used for this analysis. In general, good agreement with QCD predictions is found except for very high  $E_t$  inclusive jets.

## 1.0 Introduction

The Fermilab Tevatron Collider has recently provided a large sample of  $p\bar{p}$  collisions at a center of mass energy of 1.8 TeV from a run completed in February of 1996. These data can be used to make new, high precision tests of QCD predictions and to search for phenomena beyond those included in the Standard Model. In this report we present a study of high  $Q^2$   $p\bar{p}$  collisions by selecting events with W and Z bosons, and high  $E_t$  jets. The data were obtained using the CDF detector<sup>1)</sup>, and include 108 (106)  $\text{pb}^{-1}$  of integrated luminosity for the W (Z) production and 19.5  $\text{pb}^{-1}$  for the study of inclusive jets. Comparisons of production properties are made to QCD predictions using LO and NLO matrix element calculations as available, supplemented by simulated gluon radiation and hadronic fragmentation where appropriate.

## 2.0 The CDF Detector

The CDF tracking system, immersed in a 1.4 Tesla magnetic field, consists of a four-layer silicon strip detector (SVX) for identifying secondary decays of short lived particles, an inner wire chamber (VTX) for measurement of the interaction vertex along the beam, and a large outer drift chamber (CTC) for precision momentum measurements. The calorimeters, divided into electromagnetic and hadronic sections, are used for electron identification, jet energy measurement and missing transverse energy measurement. The central calorimeter extends out to a pseudorapidity of  $|\eta| < 1.1$ , the plug calorimeter from  $1.1 < |\eta| < 2.4$  and the forward calorimeter from  $2.2 < |\eta| < 4.2$ .

## 3.0 W and Z Boson Production

### 3.1 Introduction

Measurement of the hadronic production properties of W and Z bosons provides an opportunity to quantitatively evaluate perturbative QCD calculations at LO, NLO and NNLO. Events with Z bosons decaying to  $e^+e^-$  pairs have little background and provide an extremely clean sample of data to compare to the predictions of  $p\bar{p}$  annihilation into a weak boson plus directly radiated QCD jets. Within the context of the Standard Model there are no other sources of Z boson events, with the exception of small contributions from  $Z\gamma$ ,  $ZW$  and  $ZZ$  production. Events with W bosons decaying to  $e\nu_e$  have more background than Z events but provide about ten times the number of identified bosons. These are complicated at large jet multiplicities by contributions from top production, in addition to the small signals from  $W\gamma$ ,  $WW$  and  $WZ$  production.

The analysis presented here compares the production properties of W and Z events to QCD predictions for direct single boson production plus radiated hadronic jets. As described below the W+jets data are corrected for Standard Model predictions for top production using the measured top mass and where needed for the effect of direct photons faking jets. The strategy is to remove processes which indirectly contribute to the W or Z plus jets final state, and compare the corrected data to the QCD predictions for the direct reaction  $p\bar{p} \rightarrow W$  or  $Z$  + jets. Any deviations between the corrected data and this QCD prediction would indicate deficiencies in the calculation or evidence for physics beyond the Standard Model.

### 3.2 W and Z Boson Selection

Electron decays of the W and Z bosons are obtained from on-line triggers which require central, high transverse energy ( $E_t$ ) electrons. In the off-line analysis a central electron candidate is selected from electromagnetic calorimeter clusters with an associated track reconstructed in the CTC. Tight electron cuts are then imposed by demanding that the transverse energy in a cone of radius 0.4 in  $\eta$ - $\phi$  space around the electron cluster be less than 10% of the electron energy. The initial filter for both W and Z boson decays requires this central electron to have  $E_t \geq 20$  GeV and  $|\eta| \leq 1.1$ .

Z boson candidates are selected from events with a loosely selected second electron in the central ( $|\eta| \leq 1.1$ ), plug ( $1.1 < |\eta| \leq 2.4$ ), or forward ( $2.4 < |\eta| \leq 3.7$ ) calorimeters with  $E_t \geq 20, 15,$  or  $10$  GeV respectively. Electron candidates with photon conversion characteristics are removed, and all electrons must be separated from jets by  $\Delta R_{ej} = \sqrt{\Delta\eta^2 + \Delta\phi^2} \geq 0.52$ . A sample of 6708  $Z \rightarrow e^+e^-$  candidates are obtained after demanding opposite sign electron tracks (when well measured) and cutting on the electron invariant mass in the range  $|M_{ee} - M_Z| < 15$  GeV/ $c^2$ .

W boson candidates are selected from events with a clean central electron and missing transverse energy  $\geq 30$  GeV. A filter removing Z boson decay candidates is applied. 51431  $W \rightarrow e\nu$  decay candidates are obtained after applying all selection cuts.

Jets associated with the W and Z boson events are selected using a cone algorithm with  $R_j = 0.4$ . Jets are considered resolved if they are separated by  $\Delta R_{jj} > 1.3R_j = 0.52$ . Otherwise the two jets are merged into one. Jet corrections are made for calorimeter non-uniformities, underlying event radiation and out of cone corrections. The final selection cuts require jet  $E_t \geq 15$  GeV and  $|\eta| \leq 2.4$ . The jet multiplicity spectra associated with the selected W and Z boson candidates are presented in Table I.

### 3.3 Backgrounds to the W and Z Events

The selected sample of 6708 Z boson candidates has very low background. This is evaluated as a function of associated jet multiplicity from the invariant mass distribution of the electron pairs by extrapolating the side bands, excluding the Drell-Yan spectrum, to the mass region used for the Z boson selection. The background shape is measured from the data using non-isolated electrons. The one sigma upper limit to the background to the Z bosons increases from 1.1 to 4.0% for jet multiplicity  $\geq 0$  to 4.

The W boson background is dominated by jet production in which one jet fakes an electron. This is evaluated from the data using a two dimensional plot of electron isolation versus missing  $E_t$ , extrapolating from regions dominated by QCD events to the region used to select W boson candidates. The background varies from 3 to 27% for jet multiplicity  $\geq 0$  to 4. Smaller background contributions come from  $W \rightarrow \tau\nu$  (2%) and  $Z \rightarrow ee$  (1.5%) decays faking  $W \rightarrow e\nu$  events.

Backgrounds to the jets come from direct photons faking jets and jets from  $p\bar{p}$  collisions other than the one producing the boson. The photon background varies from 2 to 3% and the contribution of soft jets from other interactions varies from 3 to 5% for our jet selection cuts.

### 3.4 Cross sections for W and Z plus Jet Production

The W and Z data described above, corrected for backgrounds, is used to calculate the cross sections for W and Z boson production as a function of the number of associated

jets. The  $W$  and  $Z$  decays are fully corrected for trigger and electron identification efficiencies, losses due to geometric and kinematic cuts, and the effects of jets obliterating the decay electrons. The corrections are made as a function of jet multiplicity. For example the efficiencies are  $18.3 \pm 0.3\%$  for inclusive  $W$  production and  $30.1 \pm 0.6\%$  for inclusive  $Z$  production.

The cross sections are calculated as a function of jet multiplicity using the ratio of the corrected number of events with  $\geq n$  jets to the total number of events. The cross sections are determined from these ratios and the previously measured<sup>2)</sup> inclusive  $W$  and  $Z$  cross sections. For the purpose of this analysis the contribution of top production is removed from the  $W$ +jets events using the measured top mass and Standard Model predictions for top production. The results are tabulated in Table II and plotted in Figure 1. The errors quoted include statistical and systematic uncertainties added in quadrature.

The data are compared to the predictions of LO QCD (VECBOS)<sup>3)</sup> plus HERWIG<sup>4)</sup> for simulated parton showers and fragmentation to hadrons, and a selection of the jets from a CDF detector simulation. CTEQ3M parton distribution functions were used with a two-loop  $\alpha_s$  evolution. The band shows the effect of varying the renormalization and factorization scales from  $Q^2 = M^2 + p_t^2$  of the boson to the average  $p_t$  squared ( $\langle p_t \rangle^2$ ) of the partons. For  $Q^2 = M^2 + p_t^2$  the measured  $W$  and  $Z$  cross sections are about a factor of 1.7 higher than the LO QCD prediction, for all jet multiplicities. For more details see reference<sup>5)</sup>. Higher order QCD calculations have been carried out for inclusive  $W$  and  $Z$  production at NNLO<sup>5)</sup> and for  $W$  and  $Z + \geq 1$  jet production at NLO<sup>6)</sup>. Comparisons to the NLO predictions have not been completed, but the NNLO inclusive predictions are in excellent agreement with the data as discussed in reference<sup>2)</sup>.

### 3.5 Jet Production Kinematics in $W$ and $Z$ Events

The production properties of the jets and bosons are compared to LO QCD predictions using  $Q^2 = \langle p_t \rangle^2$  in the VECBOS-HERWIG generation. The simulated events are passed through the CDF detector simulation and all boson and jet cuts applied as for the data. The jet  $E_t$  spectra for the first, second and third highest  $E_t$  jets for  $\geq 1$ ,  $\geq 2$  and  $\geq 3$  jet events are shown in Figures 2 and 3 for  $Z$  and  $W$  bosons respectively. The data have been corrected for backgrounds (including  $t\bar{t}$  for the  $W$  events) and are normalized to the QCD predictions. The jet  $E_t$  spectra are in good agreement with the LO QCD predictions. The agreement between the data and LO QCD predictions is also reasonably good for other jet variables such as pseudorapidity, boson-jet scattering angle and jet-jet separation. For more details see reference<sup>5)</sup>.

## 4.0 Inclusive Jet Production

### 4.1 Introduction

$p\bar{p}$  collisions producing high  $E_t$  hadronic jets can be used to test NLO perturbative QCD calculations and to search for new physics at very small distance scales. The data presented here are from a complete analysis of  $19.5 \text{ pb}^{-1}$  of  $p\bar{p}$  collisions at  $\sqrt{s} = 1.8 \text{ TeV}$ , and a preliminary analysis of an additional  $87 \text{ pb}^{-1}$  of data. Jets are selected in the  $E_t$  range from 15 to 440 GeV, thus probing distance scales down to 0.1 milli fermi. The  $E_t$  spectrum of centrally produced jets is compared to NLO QCD predictions with a variety of parton distribution functions.

## 4.2 Jet Selection and Corrections

The data were collected using on-line triggers with jet  $E_t$  thresholds of 20, 50, 70 and 100 GeV. The lower three thresholds were prescaled by factors of 500, 20 and 6 respectively and all 100 GeV triggers were recorded. As for the W and Z events, the jets were reconstructed using a cone algorithm, but in this analysis a cone size of  $R_j = 0.7$  was used to cluster the calorimeter energy. Jets were reconstructed from the central calorimeter in a pseudorapidity range  $0.1 < |\eta| < 0.7$  where jet corrections are well understood. Underlying energy is subtracted but no out of cone corrections are applied because comparisons are made to NLO QCD predictions where these effects are included.

The measured jet  $E_t$  spectrum is corrected for detector and smearing effects caused by the  $E_t$  measurement resolution so that it can be compared directly to the NLO QCD predictions. The details of this procedure are described in reference<sup>8)</sup>. In brief, an  $E_t$  spectral function is chosen with enough parametric flexibility to represent the true jet  $E_t$  spectrum. This true spectrum is then smeared using detector response functions determined from ISAJET and Feynmann-Field jet fragmentation tuned to the CDF data. The parameters in the true spectrum are then adjusted until the smeared spectrum fits the measured CDF data. Finally, corrections are made to the measured  $E_t$  value and rate for each bin of the raw data based upon the mapping of the fitted true spectrum to the smeared spectrum. The corrected  $E_t$  data points are presented in Figure 4. The differential spectrum is averaged over the jet rapidity interval  $0.1 < |\eta| < 0.7$ . The jet production rates drops by about 9 orders of magnitude as the jet  $E_t$  increases from 15 to 440 GeV.

Systematic errors in the measured  $E_t$  spectrum have been evaluated for eight different sources: energy scale stability, high and low  $P_t$  hadron response, electron/photon response, jet fragmentation, underlying event corrections, calorimeter resolution and luminosity normalization. The effect of each of the systematic errors on the measured cross section is evaluated by varying the uncertainty by  $\pm$  one sigma and repeating the unsmearing procedure described above. The difference between the distorted  $E_t$  data point and the nominal value is determined as a function of  $E_t$  for each of the eight systematic errors. A summary of the systematic errors is presented in Figure 5.

## 4.3 Comparison of Jet $E_t$ Spectrum to NLO QCD Predictions

The QCD prediction for the di-jet production spectrum is available at a next to leading order perturbative approximation<sup>9)</sup>. A comparison of this calculation to the measured inclusive jet cross section is shown in Figure 4. The standard two-loop evolution of  $\alpha_s$  is used with a value of  $\Lambda_{\text{QCD}}$  determined by the choice of the parton distribution function (PDF). The renormalization and factorization scales were set at  $E_t/2$ . There is generally good agreement between the measured spectrum and the QCD prediction, except for very high  $E_t$  jets where the data is above the theory. The details of this disagreement depend on the choice of PDF. This is shown in more detail in Figure 6 where the percentage difference in  $(\text{data-theory})/\text{theory}$  is plotted. The solid line in Figure 4 and the comparison shown in Figure 6 uses the MRSD0' PDF. The errors on the data points are statistical and the systematic errors (added in quadrature) are displayed as the error band in Figure 6.

Various statistical tests have been used to evaluate the apparent excess of high  $E_t$  jet production. This depends on the choice of PDF. Figure 6 shows the effect of changing from MRSD0' baseline choice to 5 other PDF's. Taking into account the systematic errors,

the significance of the excess of high  $E_t$  jets in the range above 160 GeV is 1% for MRSD0' and 8% for CTEQ2M. For more details of this comparison see reference<sup>8)</sup>. Figure 7 shows a comparison of the data to QCD using CTEQ3M PDF's and includes both the  $19.5 \text{ pb}^{-1}$  of data from Tevatron Run Ia and separately an additional  $87 \text{ pb}^{-1}$  of data from Run Ib. The two data sets are statistically consistent confirming the excess of high  $E_t$  jets.

In recent months a great deal of work has been done by the CTEQ and MRS groups<sup>10)</sup> to study possible modifications of the parton distributions in the proton which could explain the observed high  $E_t$  jet excess and still be compatible with constraints imposed by precise lepton-nucleon scattering data (DIS). The conclusion of both groups is that the proton quark content is highly constrained by the DIS data and can not be modified to produce an appreciable enhancement in the high  $E_t$  inclusive jet cross section. However the high  $x$  gluon distributions are less constrained and, depending on assumptions about the  $x$  dependence of the gluon distribution, could cause an increase in the rate of high  $E_t$  jet production. For a review of these considerations see references<sup>10)</sup>. A quantitative evaluation of the agreement of the NLO QCD predictions with the measured high  $E_t$  inclusive jet spectrum will require an understanding of the high  $x$  gluon content of the proton. Additional data on di-jet angular distributions, doubly differential spectra as a function of  $E_t$  and  $\eta$ , and the  $\sqrt{s}$  dependence of the cross sections from 630 to 1800 GeV are in the process of being analyzed and will provide important added information on the overall agreement of NLO QCD predictions with high energy jet production.

## 5.0 Summary and Conclusions

A study has been made of high  $Q^2$   $p\bar{p}$  collisions at  $\sqrt{s} = 1.8 \text{ TeV}$  using the CDF detector. Events were selected with  $W$  and  $Z$  bosons plus hadronic jets, and inclusive high  $E_t$  jets. The predictions of LO QCD calculations for jet production associated with  $W$  and  $Z$  bosons agree well with the data up to an overall normalization factor of about 1.7, independent of jet multiplicity, using a renormalization/factorization scale of  $M^2 + P_t^2$  of the boson. The high  $E_t$  inclusive jet data agree with NLO QCD predictions except for jet  $E_t$  above about 200 GeV, where the measured cross section is above the theoretical predictions for a range of parton distribution functions. One possible explanation of this is an excess of high  $x$  gluons above the predictions of PDF's fit to DIS data. However other explanations, such as higher order QCD corrections, can not be excluded at this time. An understanding of high  $E_t$  jet production will be greatly improved using a more differential analysis of di-jet production at  $\sqrt{s} = 630$  and 1800 GeV, as currently being carried out by the CDF and D0 Collaborations.

## References

- [1] F. Abe *et al.*, Nucl. Instrum. Methods Phys. Res., Sect. A **271**, 387 (1988).
- [2] F. Abe *et al.*, Phys. Rev. Lett. **76**, 3070 (1996).
- [3] F. A. Berends *et al.*, Nucl. Phys. **B357**, 32 (1991).
- [4] G. Marchesini *et al.*, Comput. Phy. Commun. **67**, 465 (1992).
- [5] F. Abe *et al.*, Phys. Rev. Lett. **77**, 448 (1996).
- [6] W. L. van Neervan and E. B. Zijlstra, Nucl. Phys. **B382**, 11 (1992).
- [7] W. T. Giele, E. W. N. Glover, and D. A. Kosower, Nucl. Phys. **B403**, 633 (1993).
- [8] F. Abe *et al.*, Phys. Rev. Lett. **77**, 438 (1996).
- [9] S. Ellis *et al.*, Phys. Rev. Lett. **64**, 2121 (1990); F. Aversa *et al.*, Phys. Rev. Lett. **65**, 401 (1990); W. T. Giele *et al.*, Nucl. Phys. **B403**, 633 (1993).
- [10] J. Huston *et al.*, Phys. Rev. Lett. **77**, 444 (1996); A. D. Martin, R. G. Roberts and W. J. Sterling, preprint DTP/96/44 and RAL-TR-96-037.

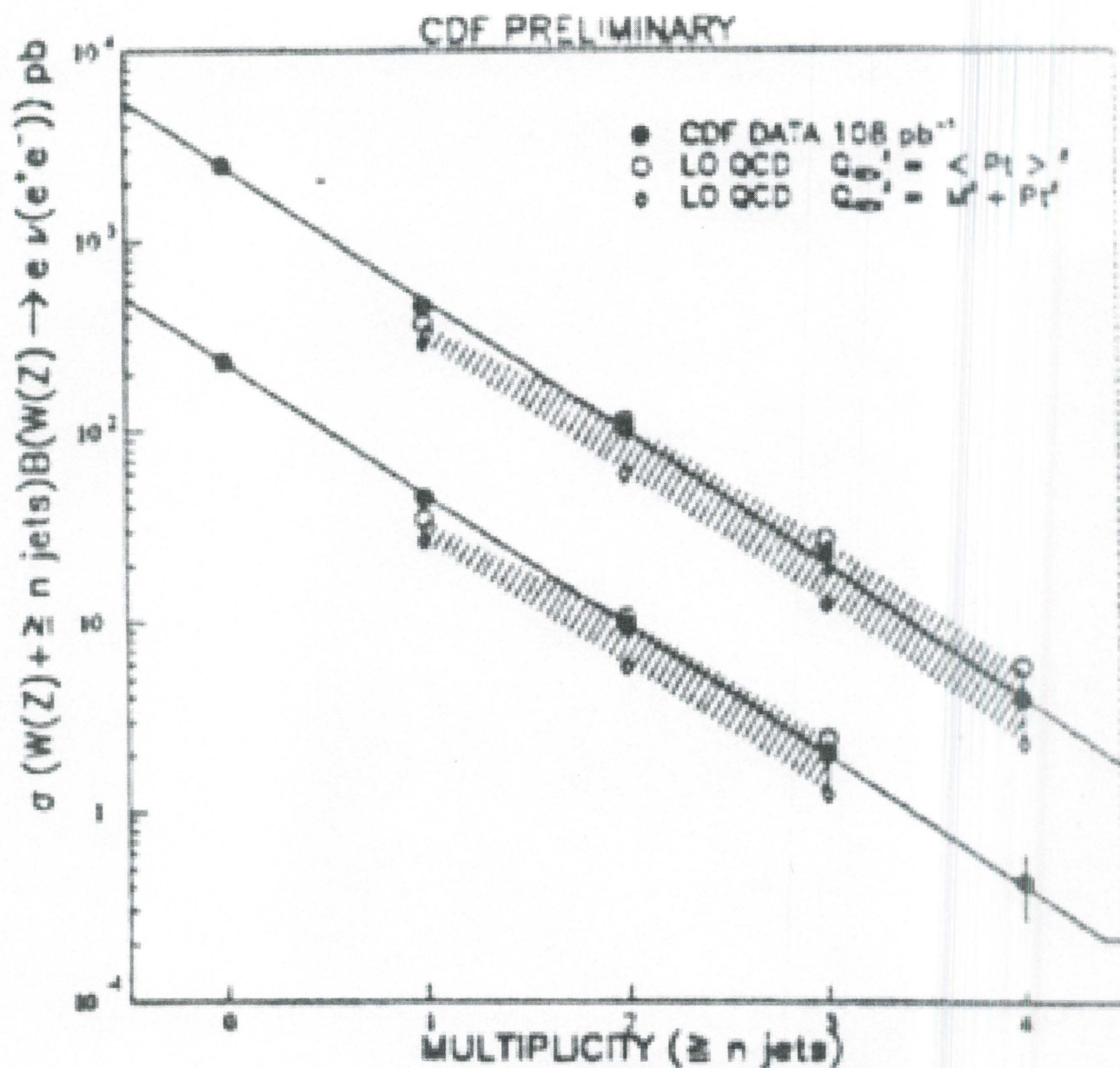


Fig. 1: Cross sections for  $W + \geq n$  jets and  $Z + \geq n$  jets for  $n = 0$  to 4. The LO QCD prediction bands span the range of renormalization scales described in the text. The error bars include both statistical and systematic errors and the lines are exponential fits to the data.

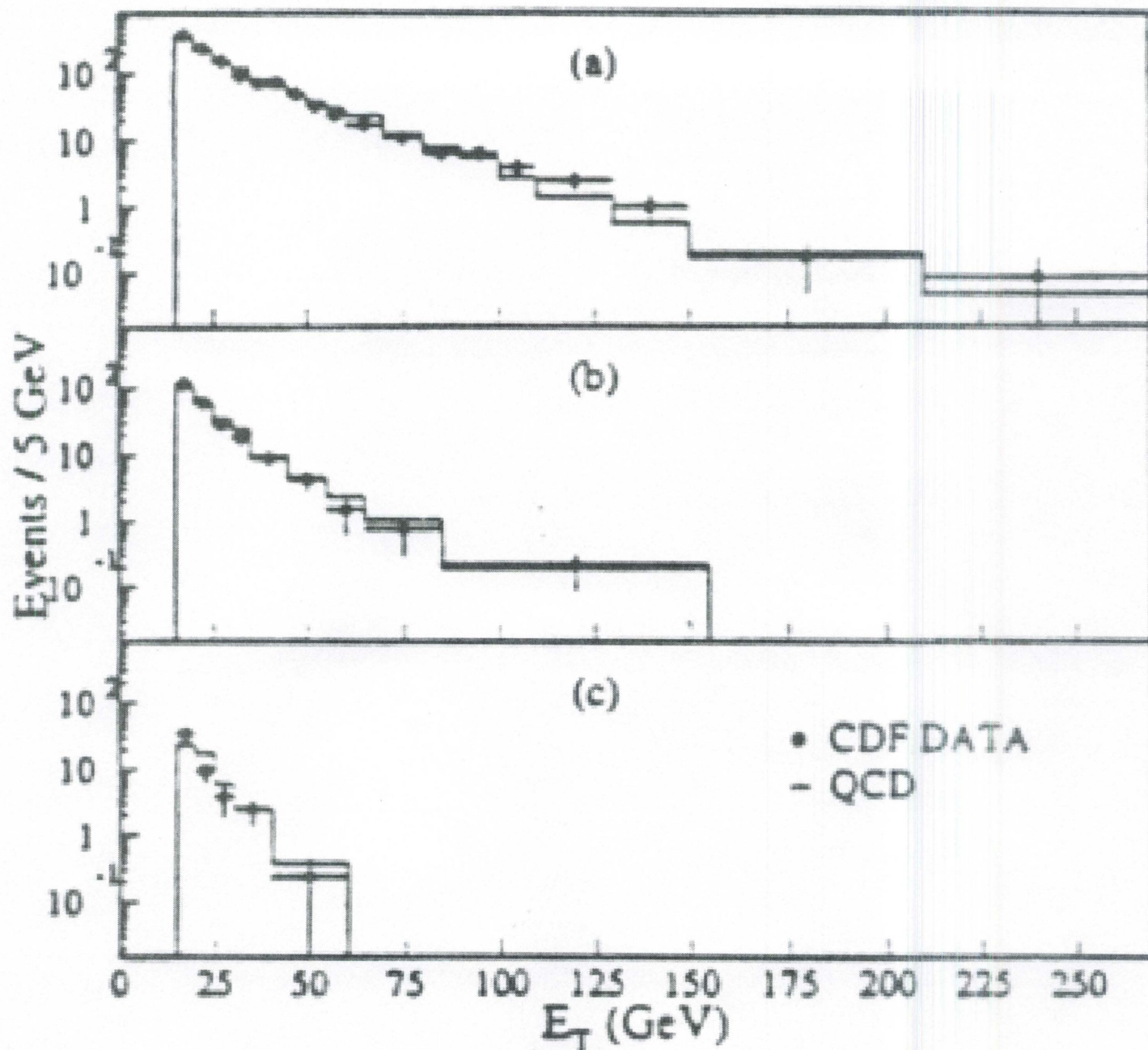


Fig. 2: Transverse energy of the (a) first, (b) second, and (c) third highest  $E_T$  jets from  $Z + \geq 1$ ,  $\geq 2$ , and  $\geq 3$  jet events. The points are the data and the histograms are the QCD predictions normalized to the data.

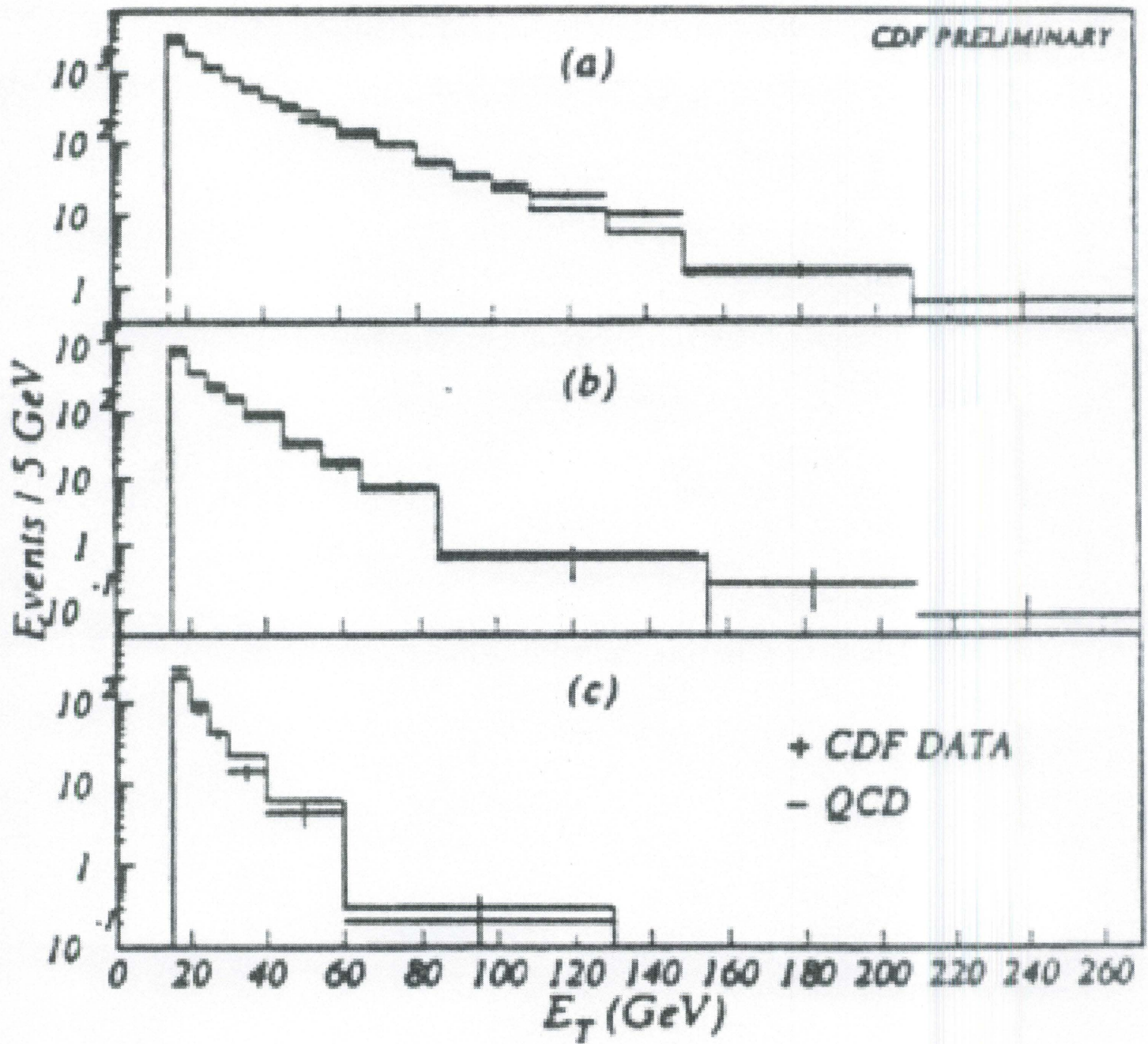


Fig. 3: Transverse energy of the (a) first, (b) second, and (c) third highest  $E_T$  jets from  $W + \geq 1$ ,  $\geq 2$ , and  $\geq 3$  jet events. The points are the data and the histograms are the QCD predictions normalized to the data.

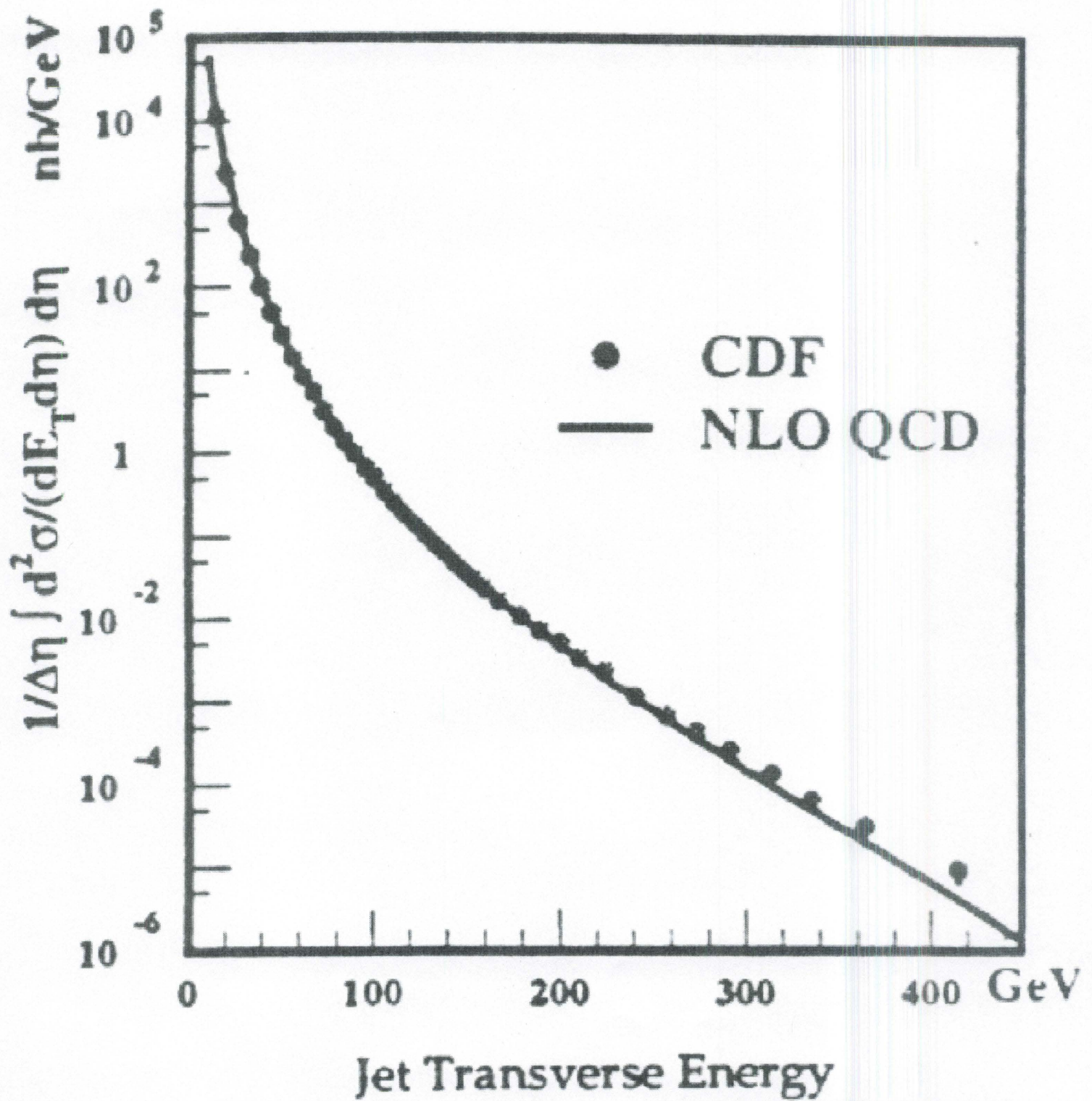


Fig. 4: The corrected inclusive jet  $E_t$  cross section compared to NLO QCD predictions using MRSD0' parton distribution functions.

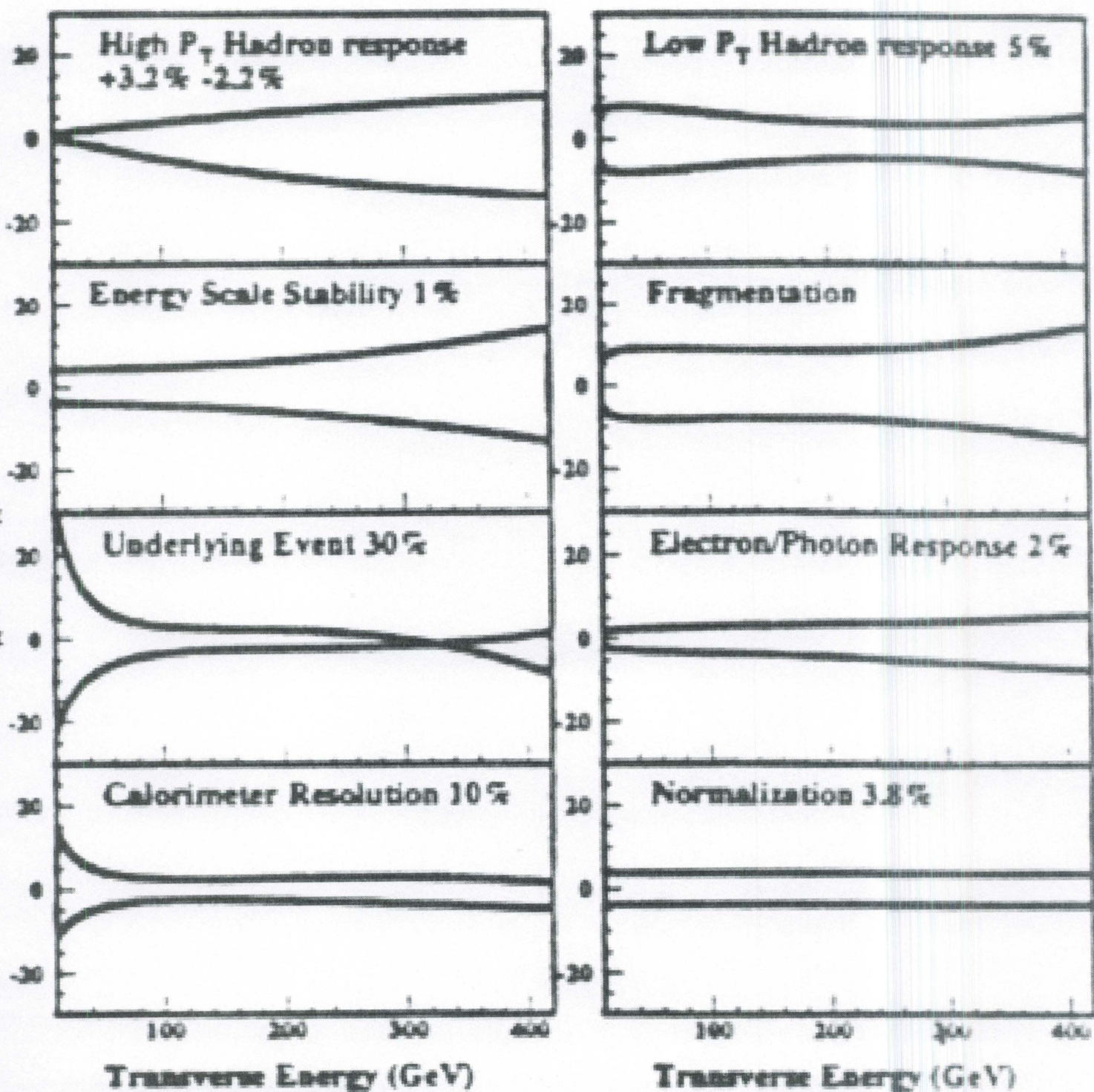


Fig. 5: The percentage change in the inclusive cross section for changes of each systematic error by  $\pm$  one sigma

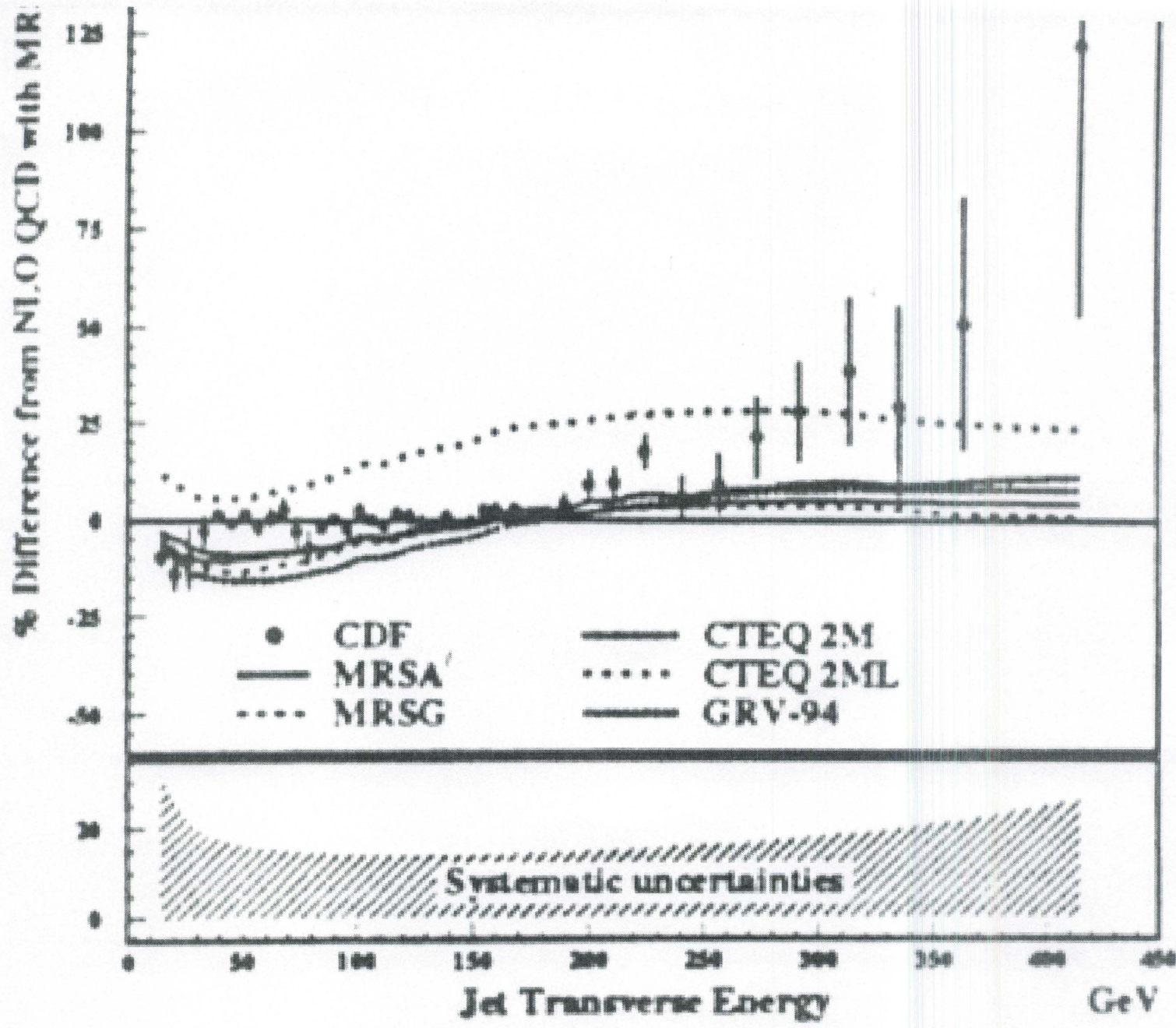


Fig. 6: The corrected inclusive jet data compared to NLO QCD predictions using MRSDO' PDF's in terms of (data-theory)/data expressed in percent (points with statistical errors). Comparisons to other PDF's is also shown. The band at the bottom of the Figure shows the

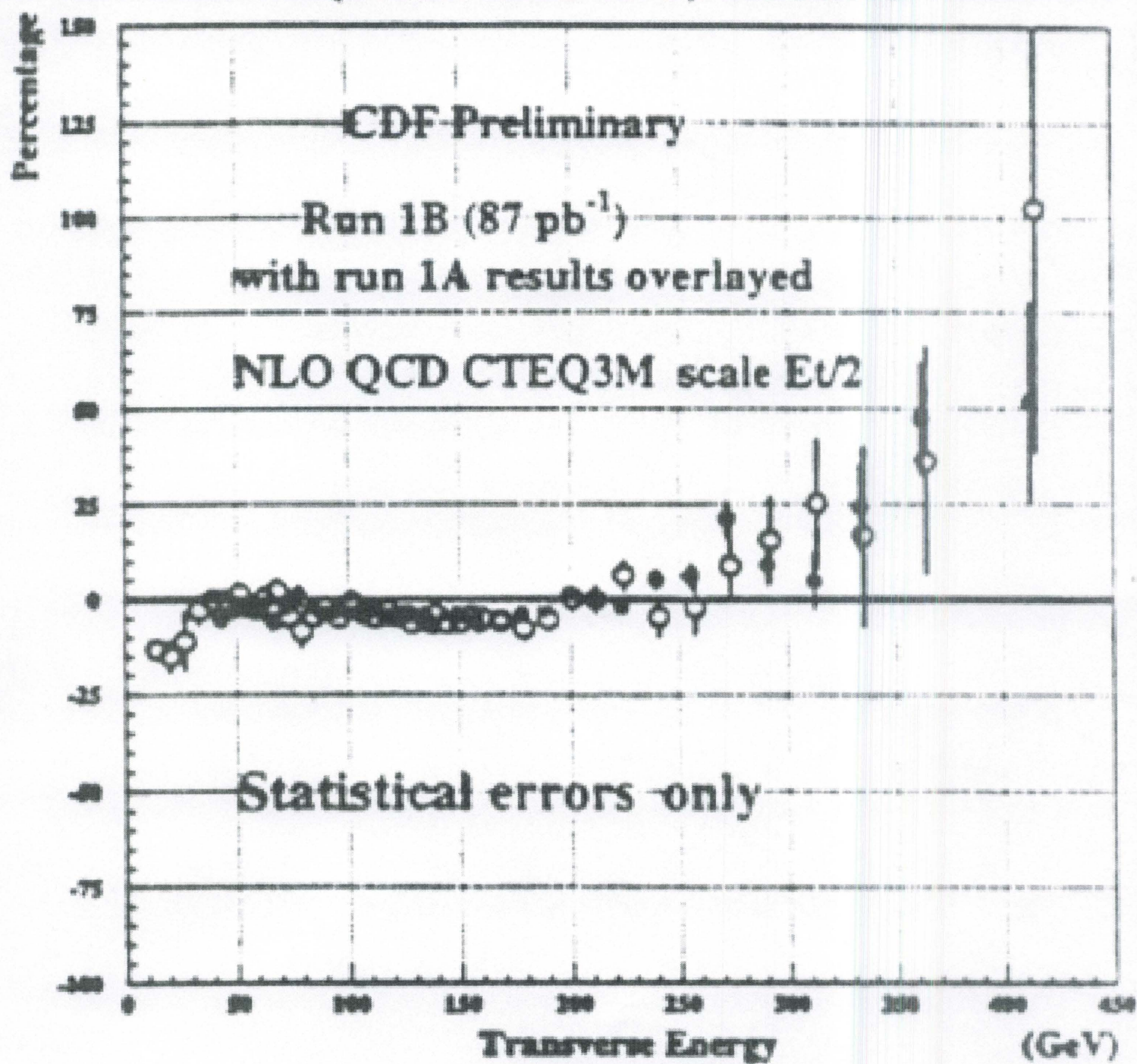


Fig. 7: The corrected inclusive jet data compared to NLO QCD predictions using CTEQ3M PDF's in terms of  $(\text{data-theory})/\text{data}$  expressed in percent (points with statistical errors). The open points are  $19.5 \text{ pb}^{-1}$  of data from Run 1a and the solid point are

$Z + \geq n$ jet events	$W + \geq n$ jet events
$n \geq 0$	$n \geq 0$
6708	51431
1	1
1310	11144
2	2
279	2596
3	3
57	580
4	4
11	126

Table I: Summary of the selected  $W \rightarrow e\nu$  and  $Z$

$\rightarrow ee$  events with the number of associated jets before background subtraction.

BRx $\sigma$ (Z + $\geq$ n jets) pb		BRx $\sigma$ (W + $\geq$ n jets) pb	
		CDF Preliminary	
n $\geq$ 0	231 $\pm$ 12.5	n $\geq$ 0	2490 $\pm$ 120
1	45.2 $\pm$ 5.8	1	458 $\pm$ 50
2	9.7 $\pm$ 1.9	2	103 $\pm$ 18
3	2.03 $\pm$ 0.56	3	22.3 $\pm$ 5.8
4	0.43 $\pm$ 0.17	4	4.0 $\pm$ 1.4

Table II: Summary of the BRx cross section for  $W \rightarrow e\nu$  and  $Z \rightarrow ee$  events. The top contribution is removed from the W cross section. The errors include both statistical and systematic uncertainties.